A Two-Stage Integrated Method for Early Prediction of Remaining Useful Life of Lithium-ion Batteries

Guijun Ma, Zidong Wang, Weibo Liu, Jingzhong Fang, Yong Zhang, Han Ding, and Ye Yuan

***Abstract*—This article puts forward a two-stage integrated method to predict the remaining useful life (RUL) of lithium-ion batteries (LIBs). At the first stage, a convolutional neural network (CNN) is employed to preliminarily estimate the cycle life of each testing LIB, where the network structure of the CNN is carefully designed to extract the discharge capacity features. By analyzing the cycle lives, an LIB which has the most similar degradation mode to each testing LIB is chosen from the training dataset. The capacities of the selected LIB are identified based on a double exponential model (DEM). At the second stage, the identified DEM is utilized as the initial mean function of the Gaussian process regression (GPR) algorithm. The GPR algorithm is then applied to early RUL prediction of each testing LIB in a personalized manner. To verify the efficacy of the proposed method, four LIBs with long-term cycle lives are selected as the testing dataset. Experimental results show the superior performance of the proposed method over the standard CNN-based RUL prediction method and the standard GPR-based RUL prediction method.**

***Index Terms*—Remaining useful life prediction, cycle life prediction, lithium-ion batteries, convolutional neural network, Gaussian process regression.**

I. Introduction

With the rapid development of electric vehicles, consumer electronics and grid energy storage systems, the global lithium-ion battery (LIB) market is expected to exceed 170 billion dollars in 2030 [34]. Along with the widespread application of LIBs, battery health management (BHM) of LIBs has gained increasing research interest from academia and industry in recent years. To develop reliable BHM techniques, an advanced battery management system needs to include several essential functions such as fault diagnosis, fault alarm, thermal management, state of charge (SOC) estimation, state of health (SOH) estimation and remaining useful life (RUL) prediction [27], [35], [42]. Among these functions, RUL prediction of LIBs aims to predict the leftover cycles that the LIBs could operate properly. An accurate prediction of RUL could improve the operation safety of LIB and provide end-users with a well-scheduled usage plan. To date, a great number of RUL prediction methods for LIBs have been developed, which can be roughly classified into three groups: 1) model-based methods, 2) data-driven methods, and 3) integrated methods [11], [18], [19], [30].

Model-based methods utilize mechanism models, equivalent circuit models (ECMs) or empirical models to investigate the degradation modes of LIBs. Mechanism models mainly consider three factors related to the internal attenuation mechanism (i.e., loss of lithium, loss of active material in the positive electrode and the negative electrode) [2], [41]. ECMs employ circuits to simplify the battery operation process, where the mapping function from ohmic/polarization resistance to capacity attenuation is established to analyze the degradation process of ECMs [26]. Empirical models like exponential models and polynomial models are easier to be constructed according to empirical degradation trend of LIB capacities [31], [51]. The adaptive filter techniques are usually employed to update the model parameters [47], [49]. Although the model-based methods have the advantage of good interpretability, these models are established by approximating the degradation mechanism, thus inevitably generating significant RUL prediction errors.

Data-driven methods could predict the RUL of LIBs by training the LIB degradation data with machine learning (ML) algorithms. Many data-driven methods have been developed to predict the RUL of each LIB in a personalized manner. The RUL of the LIB at a certain cycle can be obtained by predicting the degradation path using ML algorithms such as long short-term memory (LSTM) network [50], [52], autoregression [24], [56], relevance vector machine (RVM) [6], naive Bayes [32], convolutional neural network (CNN) [29], support vector regression (SVR) [54], Box-Cox transformation [53], and Gaussian process regression (GPR) [17], [20], [48]. With the purpose of accurate RUL prediction of LIBs, the above-mentioned data-driven methods need a great number of historical capacity data of LIBs for training, which includes the capacity data with more than 25% of total charge-discharge cycles. Unfortunately, these data-driven methods may not perform well on early RUL prediction of LIBs due to the limited capacity data.

Another kind of data-driven methods aims to perform early RUL prediction by estimating the cycle life of LIBs, where

This work was supported in part by the European Union's Horizon 2020 Research and Innovation Programme under Grant 820776 (INTEGRADDE), the Engineering and Physical Sciences Research Council (EPSRC) of the UK, the Royal Society of the UK, the Alexander von Humboldt Foundation of Germany, and the National Natural Science Foundation of China under Grant 62273264. (*Corresponding author: Zidong Wang*)

The code used in this paper is available at: `https://github.com/mxt0607/Two_Stage_RUL_Prediction`

G. Ma and H. Ding are with the School of Mechanical Science and Engineering, Huazhong University of Science and Technology, Wuhan 430074, China. (Email: `mgj@hust.edu.cn`)

Z. Wang, W. Liu and J. Fang are with the Department of Computer Science, Brunel University London, Uxbridge, Middlesex, UB8 3PH, United Kingdom. (Email: `Zidong.Wang@brunel.ac.uk`)

Y. Zhang is with the school of Information Science and Engineering, Wuhan University of Science and Technology, Wuhan 430081, China. (Email: `zhangyong77@wust.edu.cn`)

Y. Yuan is with the School of Artificial Intelligence and Automation, Huazhong University of Science and Technology, Wuhan 430074, China. (Email: `yye@hust.edu.cn`)

the cycle life is predicted for each LIB by virtue of early cycling data. For instance, the handcrafted feature (which is the variance of the discharge capacity difference between the 10th cycle and 100th cycle) have been utilized to predict the cycle lives of LIBs in a dataset with 124 LIBs by using an elastic net [38]. Based on the same dataset, a wrapper feature selection method has been developed for improving the prediction accuracy using a variety of machine learning algorithms [10]. Additionally, the dilated CNN [13] and the LSTM with attention mechanism [33] have been developed to predict the cycle lives of LIBs. Note that the above early RUL prediction methods intend to learn a global mapping function among 124 LIBs, which ignores the personalized degradation process of LIBs, thus generating relatively large prediction errors (i.e., more than 10% mean absolute percentage error).

Compared with model-based methods and data-driven methods, the goal of integrated methods is to balance the accuracy and interpretability by integrating data-driven methods and model-based methods. For example, an error compensation mechanism has been utilized in [4] to reduce LIB RUL prediction errors by combining unscented Kalman filter (UKF) with RVM based on a double exponential model (DEM), where the UKF has been employed for parameter identification of the DEM, and the RVM has been adopted for error compensation. In addition, the predicted capacity errors have been applied to update DEM parameters, where an optimized SVR has been used for error prediction, and the adaptive UKF has been employed for parameter identification [44]. Note that the aforementioned integrated methods rely on more than 35% of total charge-discharge cycles to train a reliable model, which also limits their application on RUL prediction at early cycles. Motivated by the above discussions, there is an urgent need to develop an advanced method that has satisfactory accuracy and good interpretability for early RUL prediction of LIBs.

This article puts forward a two-stage integrated method for early RUL prediction of LIBs. At the first stage, a carefully-designed CNN is utilized to preliminarily estimate the cycle life of each testing LIB. Then, one specific LIB (which has the closest cycle life to the predicted cycle life of the testing LIB) is chosen from the training dataset, and the capacities of the selected LIB are identified based on a DEM. At the second stage, an integrated strategy is employed to enhance the prediction accuracy of early RUL. To be specific, the identified DEM is adopted as the mean function of the GPR algorithm which is then trained on a small number of capacities of the testing LIB. Then, capacities in the future cycles are iteratively predicted by the trained GPR algorithm, and RUL could be calculated once the capacity reaches the failure threshold, i.e., 80% of its nominal capacity.

The main contributions of this article are summarized as follows:

1) A two-stage method is put forward for early RUL prediction of LIBs where 1) the CNN is introduced to preliminarily predict cycle lives of LIBs at the first stage; and 2) the GPR algorithm with a modified mean function is adopted for personalized RUL prediction at the second stage.
2) The structure of the CNN is designed carefully, which could effectively extract cycle life features without human intervention.
3) An integrated strategy is proposed where an identified DEM is used as the mean function of the GPR algorithm to enhance the prediction accuracy of early RUL and narrow the confidence interval of the predicted RUL.
4) The proposed two-stage integrated method is successfully verified on a well-known LIB dataset. Experimental results reveal that the proposed method is superior to the standard CNN and the standard GPR algorithm for early RUL prediction.

The remaining sections of this article are organized as follows. The background of the DEM, the CNN and the GPR algorithm are introduced in Section II. Then, a two-stage integrated method is presented for RUL prediction of LIBs. In addition, the evaluation metrics for cycle life prediction and RUL prediction are provided in this section. Section III mainly introduces the LIB dataset utilized in this paper. Section IV presents the experimental results, where the results for the first-stage cycle life prediction and the second-stage RUL prediction are discussed in detail. Finally, conclusions and some possible future research directions are provided in Section V.

II. METHODS

In this section, a brief description to the DEM, the CNN and the GPR algorithm is provided for health management of LIBs. Then, the developed two-stage integrated method is introduced with details. The performance evaluation metrics for cycle life prediction and RUL prediction of LIBs are described.

A. The DEM

The DEM, which is a nonlinear model, has been widely accepted to describe the physics-based degradation mode of LIBs by balancing the accuracy and the computational complexity [3], [44].

In this paper, the DEM is utilized to represent the LIB degradation curve. The capacity y_k of an LIB at the kth cycle is given as follows:

$$y_k = a \cdot \exp(b \cdot k) + c \cdot \exp(d \cdot k), \tag{1}$$

where a, b, c and d are the model parameters which are different for LIBs; and the symbol "$\cdot$" represents the dot product.

B. The CNN

As a popular deep learning technique, CNN has been extensively utilized in computer vision, speech processing, natural language processing, face recognition, and time-series prediction [1], [15], [25], [46]. It is known that the CNN could automatically extract implicit features from raw input and implement an "end-to-end" mapping from the raw data to the corresponding labels [7], [8], [46].

In this paper, a CNN with three convolutional modules (denoted by Conv_1, Conv_2 and Conv_3) and two fully connected

modules (represented by FC_1 and FC_2) is carefully designed for cycle life prediction of LIBs. The structure of the designed CNN is depicted in Fig. 1. To be specific, each convolutional module is constructed by one convolutional layer, one batch normalization layer [37], and the leaky rectified linear unit (Leaky ReLU) activation function in a top-down manner. Note that the max-pooling layer is only added in the first convolutional module, i.e., Conv_1). The sigmoid function is chosen as the activation function in FC_2. The Adam optimizer [14] is adopted in this paper to update weights of the CNN. The forward propagation process of the designed CNN is described by:

$$\hat{\boldsymbol{y}} = \mathrm{Sigmoid}\left(\mathrm{FC}_2\left(\mathrm{FC}_1\left(\mathrm{Conv}_3\left(\mathrm{Conv}_2\left(\mathrm{Conv}_1\left(\boldsymbol{I}\right)\right)\right)\right)\right)\right), \tag{2}$$

where $\hat{\boldsymbol{y}}$ is the predicted cycle lives of N LIBs; and $\boldsymbol{I} \in \mathbb{R}^{N\times m\times n}$ is the input data of the CNN, in which m and n are the number of utilized charge-discharge cycles of each LIB and the length of the discharge capacity data at each charge-discharge cycle, respectively.

Through stacking the above-mentioned three convolutional modules (Conv_1, Conv_2 and Conv_3), the features of the discharge capacities of LIBs could be extracted effectively. Then, two fully connected modules (FC_1 and FC_2) are employed for cycle life prediction of LIBs.

The mean square error (MSE) is utilized to measure the regression loss L_{mse}:

$$L_{\mathrm{mse}} = \frac{1}{N}\sum_{i=1}^{N}\left(y_i - \hat{y}_i\right)^2, \tag{3}$$

where $\hat{y}_i$ denotes the predicted cycle lives, and y_i is the actual cycle lives.

C. The GPR Algorithm

A GP is a collection of random variables, and any finite number of these random variables follow a joint Gaussian distribution [21]. The GPR algorithm is capable of tackling the complicated regression problem based on the GP. For an input x, the output of the GPR algorithm $y(x)$ is a GP (with a mean function $m(x)$ and a covariance function $k(x,x')$), which is shown as follows:

$$y(x) \sim \mathcal{GPR}\ (m(x),\ k(x,x')), \tag{4}$$

where x' is another input.

In this paper, $k(x,x')$ is a squared exponential (SE) covariance function given by:

$$k(x,x') = \sigma^2\ \exp\ \left(\frac{-(x-x')^2}{2l^2}\right), \tag{5}$$

where σ and l are two parameters (which are required to be optimized) for controlling the amplitude and length scales of the function, respectively.

Given a training dataset with n samples, the attribute/data set and the corresponding label set are denoted by $\boldsymbol{x} = [x_1, x_2, \ldots, x_n]$ and $\boldsymbol{y} = [y_1, y_2, \ldots, y_n]$, respectively. The joint Gaussian distribution of the training samples is described as:

$$\boldsymbol{y} \sim N(\boldsymbol{m}(\boldsymbol{x}), \mathbf{K}(\boldsymbol{x},\boldsymbol{x})), \tag{6}$$

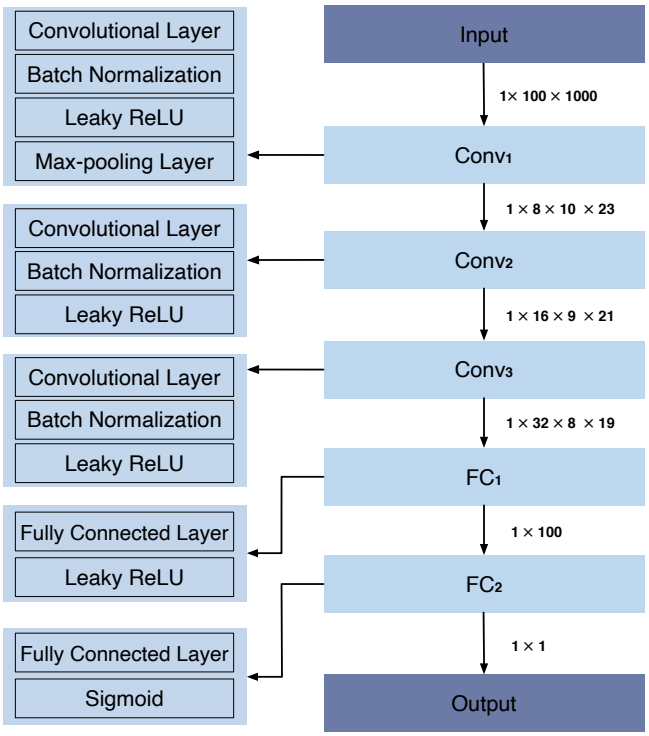

Fig. 1. The designed CNN architecture. One input sample with the shape of $1 \times 100 \times 1000$ is fed into three convolutional modules (Conv_1, Conv_2 and Conv_3) and two fully connected modules (FC_1 and FC_2) in a top-down way, where the internal layers in each module are shown in the left blocks. Moreover, the output shape of each module is marked next to the arrow.

where $\mathbf{K}(\boldsymbol{x},\boldsymbol{x}) = (k(x_i,x_j))_{n\times n}$ is a covariance matrix with each matrix element $k(x_i,x_j)$ being calculated by (5).

In the GPR algorithm, the parameters $\boldsymbol{\theta} = [\sigma, l]$ is optimized by maximizing the logarithm marginal likelihood (LML), which is given by:

$$\begin{aligned}\mathrm{LML} =\ & \ln p(\boldsymbol{y} \mid \boldsymbol{x}, \boldsymbol{\theta}) \\ =\ & \frac{1}{2}\log(\det(\mathbf{K}(\boldsymbol{x},\boldsymbol{x}))) - \frac{n}{2}\log 2\pi \\ & - \frac{1}{2}(\boldsymbol{y} - \boldsymbol{m}(\boldsymbol{x}))^T\mathbf{K}^{-1}(\boldsymbol{x},\boldsymbol{x})(\boldsymbol{y} - \boldsymbol{m}(\boldsymbol{x})),\end{aligned} \tag{7}$$

where $\det(\cdot)$ is the determinant of the square matrix "$\cdot$".

Given a testing dataset with m samples, the attribute/data set and the corresponding label set are denoted by $\boldsymbol{x}^* = [x_1^*, x_2^*, \ldots, x_p^*]$ and $\boldsymbol{y}^* = [y_1^*, y_2^*, \ldots, y_p^*]$, respectively. The training labels $\boldsymbol{y}$ and the testing labels $\boldsymbol{y}^*$ obey the following joint Gaussian distribution:

$$\begin{bmatrix}\boldsymbol{y} \\ \boldsymbol{y}^*\end{bmatrix} \sim N\left(\begin{bmatrix}\boldsymbol{m}(\boldsymbol{x}) \\ \boldsymbol{m}(\boldsymbol{x}^*)\end{bmatrix}, \begin{bmatrix}\mathbf{K}(\boldsymbol{x},\boldsymbol{x}) & \mathbf{K}(\boldsymbol{x},\boldsymbol{x}^*) \\ \mathbf{K}^T(\boldsymbol{x},\boldsymbol{x}^*) & \mathbf{K}(\boldsymbol{x}^*,\boldsymbol{x}^*)\end{bmatrix}\right). \tag{8}$$

According to (8), the predicted mean $\hat{\boldsymbol{y}}^*$ and the predicted covariance $\mathrm{cov}(\hat{\boldsymbol{y}}^*)$ can be derived as:

$$\hat{\boldsymbol{y}}^* = \boldsymbol{m}(\boldsymbol{x}^*) + \mathbf{K}^T(\boldsymbol{x},\boldsymbol{x}^*)\mathbf{K}^{-1}(\boldsymbol{x},\boldsymbol{x})(\boldsymbol{y} - \boldsymbol{m}(\boldsymbol{x})), \tag{9}$$

$$\mathrm{cov}(\hat{\boldsymbol{y}}^*) = \mathbf{K}(\boldsymbol{x}^*,\boldsymbol{x}^*) - \mathbf{K}^T(\boldsymbol{x},\boldsymbol{x}^*)\mathbf{K}^{-1}(\boldsymbol{x},\boldsymbol{x})\mathbf{K}(\boldsymbol{x},\boldsymbol{x}^*). \tag{10}$$

Generally, $\boldsymbol{m}(\boldsymbol{x}) = \mathbf{0}$ is employed when using the GPR algorithm for most prediction tasks. It should be mentioned that the DEM (described in (1)) is adopted as the mean

function $\boldsymbol{m}(\boldsymbol{x})$ for estimating the capacities of the LIBs in this article.

D. The Proposed Two-Stage Integrated Method

In this article, a two-stage integrated RUL prediction method is developed for the early prediction of LIB RUL. At the first stage, a CNN with a specifically designed network architecture is trained on the discharge capacity data and corresponding cycle lives, which is then used to predict the cycle life of each testing LIB preliminarily. Then, the LIB (which has the closest cycle life to the CNN predicted cycle life of the testing LIB) is chosen from the training dataset. The capacities of the selected LIB are identified based on a DEM. At the second stage, the identified DEM is adopted as the mean function for the GPR algorithm which is then trained based on the capacities before the end of monitoring (EOM) cycle of the testing LIB. The trained GPR algorithm is thus employed for personalized early prediction of LIB RUL at the given EOM cycle.

The procedure of the two-stage integrated method for early RUL prediction is presented as follows:

1. Preliminary cycle life prediction:
   1) Train a CNN based on the training dataset with N_1 LIBs and the validation dataset with N_2 LIBs using (2)-(3).
   2) Use the trained CNN to preliminarily estimate the cycle life of the testing LIB.
   3) Choose the LIB (which has the most similar cycle life to the CNN predicted cycle life of the testing LIB) from the training dataset.
   4) Identify the capacity curve of the selected LIB based on the DEM in (1).
2. Personalized RUL prediction:
   1) Take the DEM as the mean function of the GPR algorithm.
   2) Train the GPR algorithm using $\mathbb{D} = (k, y_k), k = 1, 2, \ldots, t_{\mathrm{EOM}}$ of the testing LIB.
   3) Predict the LIB capacities and the corresponding confidence intervals from EOM to the future cycles using (9)-(10).
   4) Calculate the RUL and its confidence interval of the testing LIB at the given EOM cycle once the predicted capacity reaches the failure threshold.

E. Evaluation Metrics

In this article, several well-known performance indicators are employed to assess the performance of the methods.

1) Evaluation Metrics for Cycle Life Prediction: At the first stage, the mean absolute percentage error (MAPE) and the root mean square error (RMSE) are chosen as the evaluation metrics for assessing the results of the cycle life prediction [38]. The MAPE denotes the average value of absolute percentage errors between the predicted cycle lives and the actual cycle lives of a certain number of LIBs. The RMSE is employed to calculate the average deviation of cycle lives. The MAPE and the RMSE are described by:

$$\mathrm{MAPE} = \frac{1}{n}\sum_{i=1}^{n}\frac{|T_i - \hat{T}_i|}{T_i} \times 100\%, \tag{11}$$

$$\mathrm{RMSE} = \sqrt{\frac{1}{n}\sum_{i=1}^{n}(T_i - \hat{T}_i)^2}, \tag{12}$$

where n is the number of testing LIBs; T_i and $\hat{T}_i$ are the actual cycle life and the predicted cycle life with respect to the ith LIB, respectively; and the symbol $|\cdot|$ denotes the absolute value.

2) Evaluation Metrics for RUL Prediction: At the second stage, three commonly-used metrics (which are the absolute error (AE), the accuracy percentage (AP), and the trend steadiness (TS)) are deployed to evaluate the RUL prediction results for one testing LIB in terms of prediction accuracy and steadiness [4], [29]. The AE is utilized to measure the deviation between the real and estimated RUL for each testing LIB. The AP is adopted to measure the percentage of the relative error for RUL prediction results. The TS is employed to assess the deviation between the predicted and actual capacities of each testing LIB. The three metrics are described as follows:

$$\mathrm{AE} = \left|T - \hat{T}\right|, \tag{13}$$

$$\mathrm{AP} = \left(1 - \frac{|T - \hat{T}|}{T}\right) \times 100\%, \tag{14}$$

$$\mathrm{TS} = \sqrt{\frac{1}{T}\sum_{i=t_{\mathrm{EOM}}+1}^{t_{\mathrm{EOM}}+T}(y_i - \hat{y}_i)^2}, \tag{15}$$

where T and $\hat{T}$ are the actual RUL and predicted RUL for the testing LIB, respectively; the symbol $|\cdot|$ is the absolute value; y_i and $\hat{y}_i$ are the actual capacity and the predicted capacity at the ith cycle, respectively; and t_{EOM} denotes the certain charge-discharge cycle which is applied to predict the LIB RUL. The prediction performance is satisfactory when the values of AE and TS are small while the value of AP is large.

III. The LIB Dataset

The utilized dataset is obtained from [38], which includes 124 lithium-iron-phosphate (LFP)/graphite LIBs. In this dataset, the nominal capacity and nominal voltage of each LIB are 1.1 Ah and 3.3 V, respectively. The cycle lives of the LIBs in this dataset are in the range of 150 to 2,300 cycles. The capacities of the LIBs are shown in Fig. 2 (a). As stated in [38], the raw dataset is divided into three parts, i.e., the training dataset (with 41 LIBs), the primary testing dataset (with 43 LIBs) and the secondary testing dataset (which includes 40 LIBs). The primary testing dataset is used to evaluate the model performance, and the secondary testing dataset (which is sampled from the utilized dataset after the model training process) is used for a rigorous test of the trained model.

All the LIBs in this dataset have been cycled under an identical discharge condition. Specifically, the LIBs have been discharged with a constant-current discharge rate of 4 C until the voltage reached 2 V, and then discharged with a constant voltage of 2 V until the current reached C/50. The fast-charging conditions are in the range of 3.6 C to 6 C. The LIBs have been tested at a constant temperature of 30 °C

in an environmental chamber. The cycle life of each LIB is the number of charge-discharge cycles when the SOH reaches 80%.

During the first-stage cycle life prediction, 26 of 41 LIBs in the training dataset are randomly selected for model training and the other 15 LIBs are chosen for model validation and model selection. Then, 43 LIBs in the primary testing dataset and 40 LIBs in the secondary testing dataset are used to evaluate the model performance.

At the second stage, four representative testing LIBs with long-term cycle lives (which are a-2, c-34, c-30 and a-9 in the two testing datasets) are employed in this paper for early prediction of LIB RUL. For ease of presentation, a-2, c-34, c-30 and a-9 (whose cycle lives are more than 900 cycles) are denoted by Cell 1, Cell 2, Cell 3 and Cell 4, respectively. The capacities of Cells 1-4 are illustrated in Fig. 2 (b). It should be noted that the discontinuous capacities of Cell 1 are attributed to a long time pause of the LIB cycling as stated in [38].

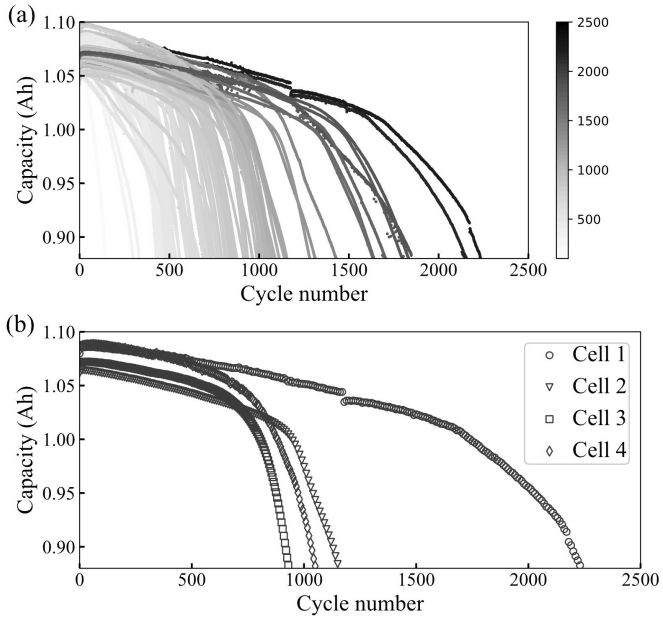

Fig. 2. (a) Capacities of 124 LFP/graphite LIBs. (b) Capacities of four testing LIBs (Cells 1-4).

IV. Results and Discussion

In this section, experimental settings are introduced, and experimental results for RUL prediction are presented. Specifically, the details of the cycle life prediction at the first stage and the RUL prediction at the second stage are introduced separately.

A. Stage 1: Cycle Life Prediction

At the first stage, the CNN is employed for cycle life prediction of LIBs. To achieve this objective, data pre-processing and data splitting are carried out in order to train a carefully-designed CNN for cycle life prediction of the testing LIBs. In the experiment, we aim to find a specific LIB from the training dataset whose degradation mode is as similar as that of the testing LIB. Note that the degradation mode of LIBs is analyzed based on the cycle life [38].

1) Experimental Setting: In the experiment, the discharge capacities and discharge voltages in each charge-discharge cycle are fitted by using a spline function, and the discharge capacities are then linearly interpolated to a certain length of 1000. The discharge capacities in the first 100 cycles of each LIB (see Fig. 3) are employed to build up a one-channel "image" with a shape of $1 \times 100 \times 1000$. Then, 26 of 41 LIBs ($\boldsymbol{I}_{\text{train}} \in \mathbb{R}^{26\times100\times1000}$) with cycle lives (which are utilized as the labels $\boldsymbol{Y}_{\text{train}} \in \mathbb{R}^{26\times1}$) are randomly chosen from the training dataset to train the CNN.

The rest 15 LIBs ($\boldsymbol{I}_{\text{val}} \in \mathbb{R}^{15\times100\times1000}$) with cycle lives (i.e., labels $\boldsymbol{Y}_{\text{val}} \in \mathbb{R}^{15\times1}$) in the training dataset are employed for model validation and model selection. In addition, all LIBs in the primary testing dataset ($\boldsymbol{I}_{\text{pr}} \in \mathbb{R}^{43\times100\times1000}$) and the secondary testing dataset ($\boldsymbol{I}_{\text{sec}} \in \mathbb{R}^{40\times100\times1000}$) are applied for cycle life prediction.

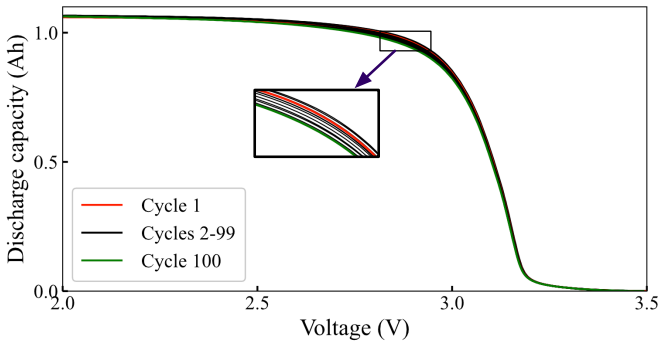

Fig. 3. The discharge capacity is a function of discharge voltage of a representative LIB.

2) Model Training: In the experiment, the input data $\boldsymbol{I}_{\text{train}}$ and the labels $\boldsymbol{Y}_{\text{train}}$ are employed to train the CNN. The network architecture of the CNN is depicted in Fig. 1, and the parameters of the CNN are presented in Table I. To facilitate the convolutional operation, the number of convolutional kernels in three convolutional layers are set to be 8, 16 and 32, respectively. The kernel size and stride in each convolutional layer or the max-pooling layer are empirically chosen. The number of neurons in the fully connected layers (which are in FC_1 and FC_2) are set to be 100 and 1, respectively. The slopes of all Leaky ReLU activation functions are set as 0.1 by default. The sigmoid activation function is adopted in the output layer. The maximum number of training epoch is set to be 1000.

During the training process, the CNN is evaluated on the validation dataset with the input $\boldsymbol{I}_{\text{val}}$ and the labels $\boldsymbol{Y}_{\text{val}}$ so as to optimize the CNN with the minimum validation error. The Adam optimizer [14] with a learning rate of 1e-5 is applied to update the weights.

3) Cycle Life Prediction of LIBs: Experimental results of cycle life prediction for the primary and the secondary testing datasets are illustrated in Fig. 4. The RMSE and the MAPE results are displayed in Table II. As shown in Table II, RMSE and MAPE (see (11)-(12)) are used for performance evaluation

TABLE I
PARAMETER SETTING OF THE CNN

Module	Layer	Kernels/Nodes	Slope	Kernel size/Stride	Output size
Input	Input	-	-	-	1×100×1000
Conv_1	Convolutional layer	8	-	(50,50)/(5,40)	1×8×11×24
	Batch normalization	8	-	-	1×8×11×24
	Leaky ReLU	-	0.1	-	1×8×11×24
	Max-pooling layer	-	-	(2,2)/(1,1)	1×8×10×23
Conv_2	Convolutional layer	16	-	(2,3)/(1,1)	1×16×9×21
	Batch normalization	16	-	-	1×16×9×21
	Leaky ReLU	-	0.1	-	1×16×9×21
Conv_3	Convolutional layer	32	-	(2,3)/(1,1)	1×32×8×19
	Batch normalization	32	-	-	1×32×8×19
	Leaky ReLU	-	0.1	-	1×32×8×19
Flatten	Flatten	-	-	-	1×4864
FC_1	Fully connected layer	100	-	-	1×100
	Leaky ReLU	-	0.1	-	1×100
FC_2	Fully connected layer	1	-	-	1×1
(Output)	Sigmoid	-	-	-	1×1

on cycle life prediction, where the RMSEs of our method on the primary and the secondary testing datasets are 90 cycles and 160 cycles, respectively. The MAPEs of our method on the primary and the secondary testing datasets are 10% and 11.7%, respectively.

To verify the effectiveness of our model, the cycle life prediction results stated in [38] are utilized as the benchmark. It should be mentioned that the approach proposed in [38] combines the handcrafted features with an elastic net for cycle life prediction. As displayed in Table II, the prediction error of our method is smaller than that of the benchmark method, which demonstrates the superiority of our method.

4) Degradation Mode Identification of Chosen LIBs: By analyzing the predicted cycle life of each testing cell, the most similar LIB (which has the closest cycle life) is chosen from the training dataset, which indicates that the selected LIB has similar degradation mode to the testing LIB. The capacities of Cells 1-4 and the chosen LIBs in the training dataset are displayed in Fig. 5. The actual cycle lives and predicted cycle lives of Cells 1-4 as well as the four selected LIBs are presented in Table III. In Table III, the predicted cycle life of Cell 1 is 2092 cycles, and the chosen LIB in the training dataset is a-1 whose actual cycle life is 2157 cycles. Thus, the capacities of a-1 are adopted as the initial capacities of Cell 1 for further RUL prediction.

Based on the DEM defined in (1), the model parameters are determined by using a MATLAB curve fitting tool to analyze the capacity data. The fitting results of the four LIBs are shown in Fig. 6. The identified DEM parameters $[a; b; c; d] \in \mathbb{R}^{4\times 1}$ are recorded in Table IV.

B. Stage 2: RUL Prediction

This section presents the experimental setting of the personalized RUL prediction method and demonstrates the RUL prediction results on Cells 1-4.

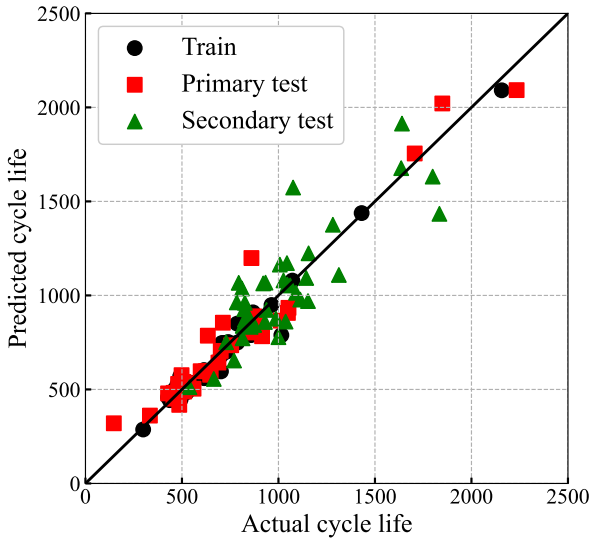

Fig. 4. The actual cycle life versus the predicted cycle lives for the training dataset, the primary testing dataset and the secondary testing dataset. The training data are used to train the CNN model parameters. The primary testing dataset is used to verify the performance of the trained CNN, and the secondary testing dataset is used to further evaluate the effectiveness of the trained CNN.

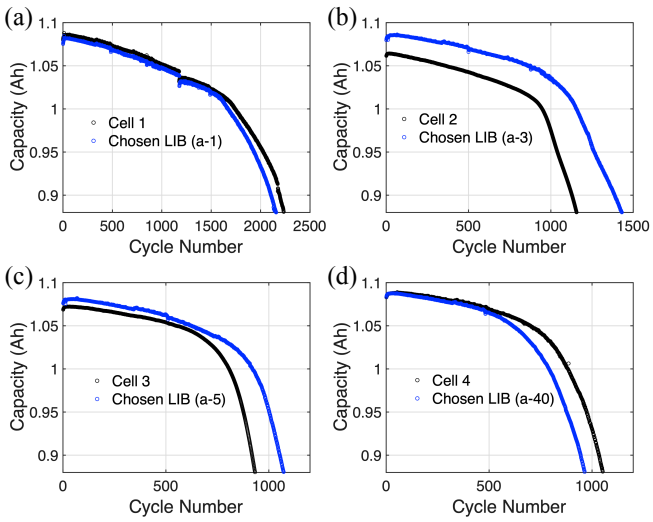

Fig. 5. The capacities of Cells 1-4 and the selected training LIBs.

1) Experimental Setting: The input data and output labels of the GPR algorithm are the cycle numbers and the capacities of the testing LIBs, respectively. Notice that the input of the GPR algorithm for training is a d-dimensional vector where d is the value of EOM. In this experiment, EOM is set to be three early cycle numbers, i.e., 200, 300 and 500. The main objective of this stage is to predict the capacities of the LIB within a certain time period according to the corresponding cycle numbers (which are larger than the EOM value). Thus, the RUL of the LIB is calculated when the predicted capacity of this LIB reaches the end of life (EOL), i.e., 0.88 Ah.

2) Model Training: By taking the identified DEM as the initial mean function of the GPR algorithm, the capacities of a testing LIB at early cycles are adopted to train the GPR

TABLE II
RMSE AND MAPE FOR CYCLE LIFE PREDICTION

	RMSE (cycles)			MAPE (%)		
	Train	Primary test	Secondary test	Train	Primary test	Secondary test
Severson *et al.* [38]	51	91	173	5.6	13	**8.6**
CNN model (Ours)	**51**	**90**	**160**	**5.1**	**10**	11.7

TABLE III
ACTUAL CYCLE LIVES, PREDICTED CYCLE LIVES AND CHOSEN LIBS FOR CELLS 1-4

	Cell 1	Cell 2	Cell 3	Cell 4
Actual cycle life	2234	1156	933	1052
Predicted cycle life	2092	1224	1068	934
Chosen LIB	a-1 (2157)	a-3 (1431)	a-5 (1072)	a-40 (964)

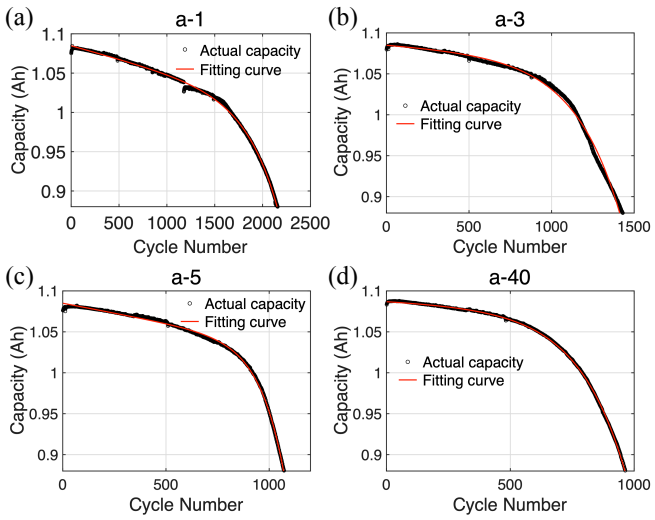

Fig. 6. Fitting curves of four chosen LIBs.

TABLE IV
IDENTIFIED DEM PARAMETERS OF THE CHOSEN LIBS FOR CELLS 1-4

Testing LIB	Chosen LIB	DEM parameters
Cell 1	a-1	[-0.0002079; 0.003009; 1.085; -3.117e-05]
Cell 2	a-3	[-0.001105; 0.003635; 1.086; -1.223e-05]
Cell 3	a-5	[-1.634e-05; 0.008557; 1.085; -4.489e-05]
Cell 4	a-40	[-0.00119; 0.0053; 1.088; -1.202e-05]

algorithm before the EOM cycle. Then, the obtained GPR algorithm is used to predict the RUL of the testing LIB at the EOM cycle.

In this paper, a bias term e is added into the mean function (see (1)), which is given by:

$$y_k = a \cdot \exp(b \cdot k) + c \cdot \exp(d \cdot k) + e. \quad (16)$$

As shown in Fig. 6, there exists a bias between the testing LIBs and their corresponding LIBs selected from the training dataset. The introduction of the bias term could contribute to the training of the GPR algorithm, which improves the flexibility of the GPR algorithm.

TABLE V
EVALUATION METRICS FOR DIFFERENT METHODS AND DIFFERENT EOM CYCLES

LIB	EOM	Methods	Predicted RUL	Actual RUL	AE	AP	TS
Cell 1	200	CNN alone	1892	2034	142	93.019%	-
		GPR w/o prior	907	2034	1127	44.592%	0.3358
		GPR w/o bias	1894±31	2034	140±31	93.117%±1.524%	0.0238
		Ours	1938±28	2034	**96±28**	**95.280%±1.377%**	**0.0156**
	300	CNN alone	1792	1934	142	92.658%	-
		GPR w/o prior	1428	1934	506	73.837%	0.0883
		GPR w/o bias	1753±24	1934	181±24	90.641%±1.241%	0.0331
		Ours	1874±19	1934	**60±19**	**96.898%±0.982%**	**0.0098**
	500	CNN alone	1592	1734	142	91.811%	-
		GPR w/o prior	957	1734	777	55.190%	0.3819
		GPR w/o bias	1614±24	1734	120±24	93.080%±1.384%	0.0217
		Ours	1683±10	1734	**51±10**	**97.059%±0.577%**	**0.0086**
Cell 2	200	CNN alone	1024	956	**68**	**92.887%**	-
		GPR w/o prior	1067	956	111	88.389%	0.0240
		GPR w/o bias	1255±84	956	299±84	68.724%±8.787%	0.0498
		Ours	1050±24	956	94±24	90.167%±2.511%	**0.0130**
	300	CNN alone	924	856	68	92.056%	-
		GPR w/o prior	1510	856	654	23.598%	0.0272
		GPR w/o bias	1135±78	856	279±78	67.407%±9.112%	0.0500
		Ours	870±24	856	**14±24**	**98.365%±2.804%**	**0.0107**
	500	CNN alone	724	656	68	89.634%	-
		GPR w/o prior	1555	656	899	-37.043%	0.0359
		GPR w/o bias	935±78	656	279±78	57.470%±11.890%	0.0545
		Ours	614±14	656	**42±14**	**93.598%±2.134%**	**0.0248**
Cell 3	200	CNN alone	868	733	135	81.583%	-
		GPR w/o prior	885	733	152	79.263%	0.0245
		GPR w/o bias	819±22	733	86±22	88.267%±3.001%	0.0223
		Ours	756±5	733	**23±5**	**96.862%±0.682%**	**0.0075**
	300	CNN alone	768	633	135	78.673%	-
		GPR w/o prior	571	633	62	90.205%	0.0381
		GPR w/o bias	776±2	633	143±2	77.409%±0.316%	0.0341
		Ours	656±4	633	**23±4**	**96.367%±0.632%**	**0.0075**
	500	CNN alone	568	433	135	68.822%	-
		GPR w/o prior	485	433	52	87.991%	0.0106
		GPR w/o bias	389±1	433	44±1	89.838%±0.231%	0.0319
		Ours	435±4	433	**2±4**	**99.538%±0.924%**	**0.0083**
Cell 4	200	CNN alone	734	852	118	86.150%	-
		GPR w/o prior	765	852	**87**	**89.789%**	0.0546
		GPR w/o bias	724±6	852	128±22	84.977%±0.704%	0.0660
		Ours	748±7	852	104±7	87.793%±0.822%	**0.0499**
	300	CNN alone	634	752	118	84.309%	-
		GPR w/o prior	602	752	150	80.053%	0.0903
		GPR w/o bias	663±2	752	89±2	88.165%±0.266%	0.0440
		Ours	725±2	752	**27±2**	**96.410%±0.266%**	**0.0123**
	500	CNN alone	434	552	118	78.623%	-
		GPR w/o prior	367	552	185	66.486%	0.1355
		GPR w/o bias	463±2	552	89±2	83.877%±0.362%	0.0514
		Ours	558±3	552	**6±3**	**98.913%±0.544%**	**0.0019**

3) RUL Prediction: In this paper, RUL is an estimation of the leftover charge-discharge cycles that a cell would operate

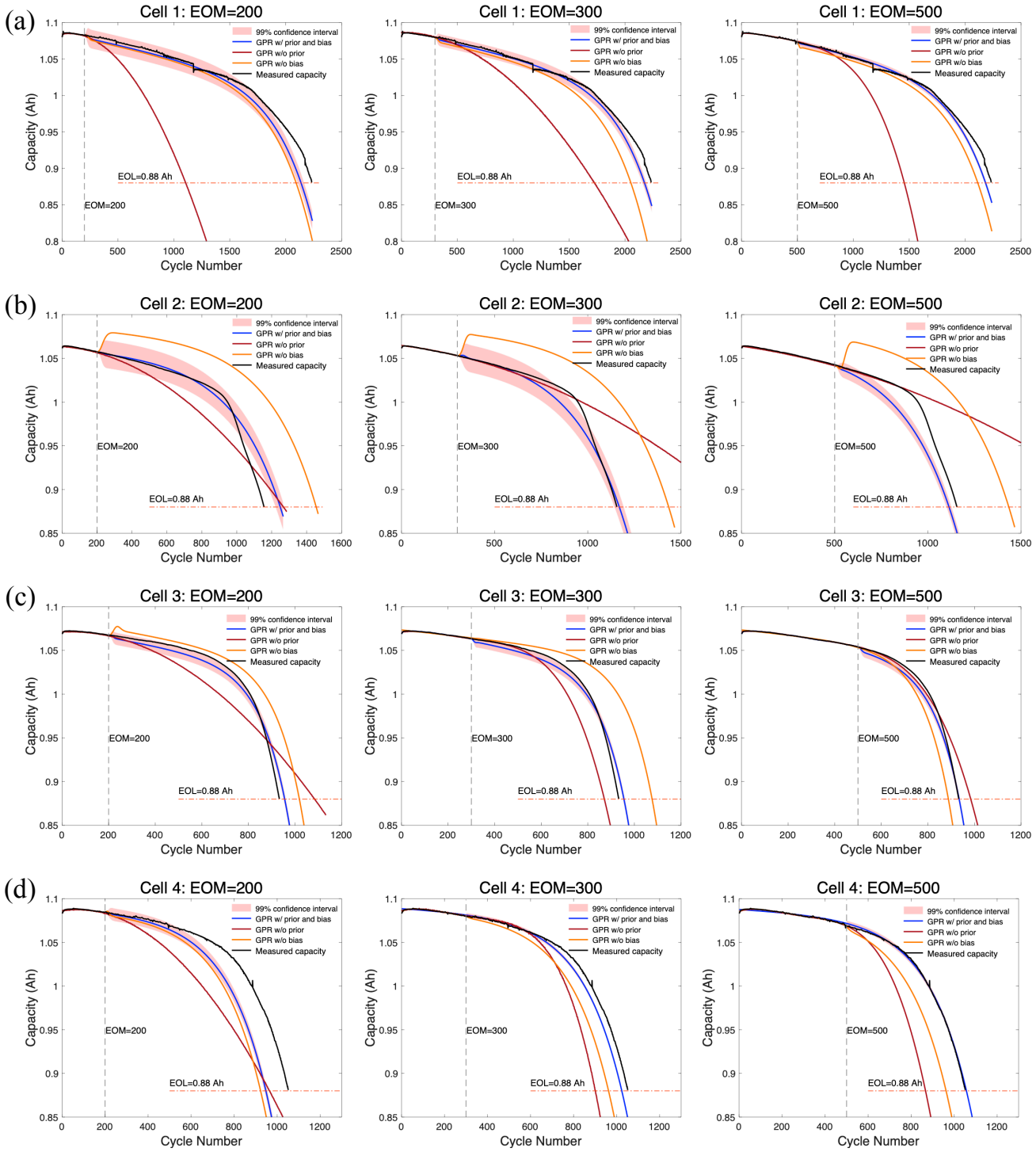

Fig. 7. Predicted capacities for (a) Cell 1, (b) Cell 2, (c) Cell 3 and (d) Cell 4. For each testing LIB, EOM cycles of 200, 300 and 500 are used to test the prediction performance. Two benchmark methods, the GPR algorithm without an initial mean function (denoted by GPR w/o prior) and the GPR algorithm without a bias term (denoted by GPR w/o bias), are used to compare with the proposed approach. RULs are calculated when the predicted capacity reaches the EOL.

successfully. By predicting the battery capacities after the EOM cycle using the GPR algorithm, RUL can be calculated by the difference between the EOM cycle and the failure charge-discharge cycle (which is the cycle number when the predicted capacity reaches the EOL).

The performance of the proposed two-stage integrated method for RUL prediction is evaluated on Cells 1-4. In this paper, the standard CNN (denoted by CNN alone), the GPR algorithm without an initial mean function (denoted by GPR w/o prior) and the GPR algorithm without the bias term (denoted by GPR w/o bias) are adopted for comparison. It should be pointed out that the designed CNN utilizes the prediction results of cycle life at the first stage, where the

predicted RUL at the EOM cycle is the difference between the predicted cycle life and the EOM cycle. By using the GPR algorithm, the predicted capacities and the corresponding 99% confidence intervals for Cells 1-4 are displayed in Fig. 7. The RUL prediction results of the selected methods are recorded in Table V, where AE, AP and TS (see (13)-(15)) are employed for performance evaluation.

For ease of presentation, let us take Cell 1 with an EOM cycle of 200 as an example. Fig. 7 (a) displays the prediction results of the capacities for Cell 1, where the predicted capacities and corresponding confidence intervals are both presented. As shown in Table V, the AE, AP and TS of the proposed two-stage integrated method are 96$\pm$28 cycles, 95.280%$\pm$1.377% and 0.0156 Ah, respectively. The standard CNN obtains the AE of 142 cycles and the AP of 93.019%. The confidence intervals are not provided because the standard CNN is a point-wise estimation method, and the TS is unavailable because the standard CNN can only predict the cycle life of LIBs. Compared with the standard CNN, the proposed method could predict the RUL for each LIB in a personalized way, thus effectively improving the RUL prediction accuracy on each individual LIB.

As given in Table V, the AE, AP and TS of the GPR w/o prior are 1127 cycles, 44.592% and 0.03358 Ah, respectively. The AE, AP and TS of the GPR w/o bias are 140$\pm$31 cycles, 93.117%$\pm$1.524% and 0.0238 Ah, respectively. The confidence intervals predicted by GPR w/o prior are too large to be quantified, which are not presented in this paper. Compared with the GPR w/o prior, the proposed approach exhibits smaller prediction errors for both RUL prediction and confidence interval prediction, which demonstrates that the DEM-based mean function could benefit the capacity prediction process. In addition, our approach outperforms the GPR w/o bias owing to the introduction of the bias term which makes the GPR training process more flexible.

Motivated by above discussions, we can conclude that our method demonstrates superior performance over the baselines on Cell 1 with an EOM cycle of 200. Likewise, we could obtain similar results on Cells 2-4 with different settings of EOM cycles, which further verifies the effectiveness of our method on early RUL prediction of LIBs.

V. Conclusion

In this article, a two-stage integrated method has been put forward for early RUL prediction of LIBs, where a CNN with designed network structure has been applied to cycle life prediction, and the GPR algorithm has been utilized to estimate the RUL of LIB in a personalized manner. At the cycle life prediction stage, a specific LIB (whose cycle life is the most similar to the predicted one of the testing LIB) has been chosen from the training dataset for identifying the DEM based on the capacity data. At the RUL prediction stage, the identified DEM has been utilized as the initial mean function for the GPR algorithm. Then, the GPR algorithm has been trained based on the capacity data of each testing LIB (with only a small number of charge-discharge cycles) for early RUL prediction. The proposed early prediction method has been successfully exploited in four selected long-cycle-life LIBs for personalized RUL prediction. Experimental results have revealed that the two-stage integrated method outperforms the benchmark methods in terms of the RUL prediction accuracy. In the future, we aim to 1) apply the proposed method to RUL prediction of other batteries; 2) employ evolutionary computation methods to optimize the hyperparameters of the proposed method [9], [22], [23], [39], [40], [43]; 3) use some up-to-date filtering and state estimation algorithms for cycle life prediction of LIBs and build reliable BHM systems [5], [12], [16], [36], [45], [55].

References

[1] L. Alzubaidi, J. Zhang, A. J. Humaidi, A. Al-Dujaili, Y. Duan, O. Al-Shamma, J. Santamaría, M. A. Fadhel, M. Al-Amidie, and L. Farhan, Review of deep learning: Concepts, CNN architectures, challenges, applications, future directions, *Journal of Big Data*, vol. 8, art. no. 53, 2021.

[2] C. R. Birkl, M. R. Roberts, E. McTurk, P. G. Bruce, and D. A. Howey, Degradation diagnostics for lithium ion cells, *Journal of Power Sources*, vol. 341, pp. 373-386, 2017.

[3] M. Catelani, L. Ciani, R. Fantacci, G. Patrizi, and B. Picano, Remaining useful life estimation for prognostics of lithium-ion batteries based on recurrent neural network, *IEEE Transactions on Instrumentation and Measurement*, vol. 70, art. no. 3524611, 2021.

[4] Y. Chang, H. Fang, and Y. Zhang, A new hybrid method for the prediction of the remaining useful life of a lithium-ion battery, *Applied Energy*, vol. 206, pp. 1564-1578, 2017.

[5] J. Chen, X. Luo, Y. Yuan, M. Shang, M. Zhong, and X. Zhang, Performance of latent factor models with extended linear biases, *Knowledge-Based Systems*, vol. 123, pp. 128-136, 2017.

[6] Z. Chen, N. Shi, Y. Ji, M. Niu, and Y. Wang, Lithium-ion batteries remaining useful life prediction based on BLS-RVM, *Energy*, vol. 234, art. no. 121269, 2021.

[7] C. Cheng, G. Ma, Y. Zhang, M. Sun, F. Teng, H. Ding, and Y. Yuan, A deep learning-based remaining useful life prediction approach for bearings, *IEEE/ASME Transactions on Mechatronics*, vol. 25, no. 3, pp. 1243-1254, 2020.

[8] C. Cheng, B. Zhou, G. Ma, D. Wu, and Y. Yuan, Wasserstein distance based deep adversarial transfer learning for intelligent fault diagnosis with unlabeled or insufficient labeled data, *Neurocomputing*, vol. 409, pp. 35-45, 2020.

[9] H. Cheng, Z. Wang, L. Ma, X. Liu, and Z. Wei, Multi-task pruning via filter index sharing: A many-objective optimization approach, *Cognitive Computation*, vol. 13, no. 4, pp. 1070-1084, 2021.

[10] Z. Fei, F. Yang, K.-L. Tsui, L. Li, and Z. Zhang, Early prediction of battery lifetime via a machine learning based framework, *Energy*, vol. 225, art. no. 120205, 2021.

[11] M.-F. Ge, Y. Liu, X. Jiang, and J. Liu, A review on state of health estimations and remaining useful life prognostics of lithium-ion batteries, *Measurement*, vol. 174, art. no. 109057, 2021.

[12] H. Geng, H. Liu, L. Ma, and X. Yi, Multi-sensor filtering fusion meets censored measurements under a constrained network environment: Advances, challenges and prospects, *International Journal of Systems Science*, vol. 52, no. 16, pp. 3410-3436, 2021.

[13] J. Hong, D. Lee, E.-R. Jeong, and Y. Yi, Towards the swift prediction of the remaining useful life of lithium-ion batteries with end-to-end deep learning, *Applied energy*, vol. 278, art. no. 115646, 2020.

[14] D. P. Kingma and J. Ba, Adam: A method for stochastic optimization, *preprint arXiv: 1412.6980*, 2014.

[15] J. Li, W. Xu, L. Deng, Y. Xiao, Z. Han, and H. Zheng, Deep learning for visual recognition and detection of aquatic animals: A review, *Reviews in Aquaculture*, in press, DOI: 10.1111/raq.12726.

[16] X. Li, Q. Song, Z. Zhao, Y. Liu, and F. E. Alsaadi, Optimal control and zero-sum differential game for Hurwicz model considering singular systems with multifactor and uncertainty, *International Journal of Systems Science*, vol. 53, no. 7, pp. 1416-1435, 2022.

[17] X. Li, Z. Wang, and J. Yan, Prognostic health condition for lithium battery using the partial incremental capacity and Gaussian process regression, *Journal of Power Sources*, vol. 421, pp. 56-67, 2019.

[18] Y. Li, K. Liu, A. M. Foley, A. Zülke, M. Berecibar, E. Nanini-Maury, J. Van Mierlo, and H. E. Hoster, Data-driven health estimation and lifetime prediction of lithium-ion batteries: A review, *Renewable and Sustainable Energy Reviews*, vol. 113, art. no. 109254, 2019.

[19] M. H. Lipu, M. Hannan, A. Hussain, M. Hoque, P. J. Ker, M. M. Saad, and A. Ayob, A review of state of health and remaining useful life estimation methods for lithium-ion battery in electric vehicles: Challenges and recommendations, *Journal of Cleaner Production*, vol. 205, pp. 115-133, 2018.

[20] K. Liu, Y. Li, X. Hu, M. Lucu, and W. D. Widanage, Gaussian process regression with automatic relevance determination kernel for calendar aging prediction of lithium-ion batteries, *IEEE Transactions on Industrial Informatics*, vol. 16, no. 6, pp. 3767-3777, 2019.

[21] K. Liu, X. Tang, R. Teodorescu, F. Gao, and J. Meng, Future ageing trajectory prediction for lithium-ion battery considering the knee point effect, *IEEE Transactions on Energy Conversion*, vol. 37, no. 2, pp. 1282-1291, 2021.

[22] W. Liu, Z. Wang, Y. Yuan, N. Zeng, K. Hone, and X. Liu, A novel sigmoid-function-based adaptive weighted particle swarm optimizer, *IEEE Transactions on Cybernetics*, vol. 51, no. 2, pp. 1085-1093, 2021.

[23] W. Liu, Z. Wang, N. Zeng, Y. Yuan, F. E. Alsasdi, and X. Liu, A novel randomised particle swarm optimizer, *International Journal of Machine Learning and Cybernetics*, vol. 12, no. 2, pp. 529-540, 2021.

[24] B. Long, W. Xian, L. Jiang, and Z. Liu, An improved autoregressive model by particle swarm optimization for prognostics of lithium-ion batteries, *Microelectronics Reliability*, vol. 53, no. 6, pp. 821-831, 2013.

[25] P. Lu, B. Song, and L. Xu, Human face recognition based on convolutional neural network and augmented dataset, *Systems Science & Control Engineering*, vol. 9, no. s2, pp. 29-37, 2021.

[26] Z. Lyu, R. Gao, and L. Chen, Li-ion battery state of health estimation and remaining useful life prediction through a model-data-fusion method, *IEEE Transactions on Power Electronics*, vol. 36, no. 6, pp. 6228-6240, 2020.

[27] G. Ma, S. Xu, and C. Cheng, Fault detection of lithium-ion battery packs with a graph-based method, *Journal of Energy Storage*, vol. 43, art. no. 103209, 2021.

[28] G. Ma, S. Xu, T. Yang, Z. Du, L. Zhu, H. Ding, and Y. Yuan, A transfer learning-based method for personalized state of health estimation of lithium-ion batteries, *IEEE Transactions on Neural Networks and Learning Systems*, in press, DOI: 10.1109/TNNLS.2022.3176925.

[29] G. Ma, Y. Zhang, C. Cheng, B. Zhou, P. Hu, and Y. Yuan, Remaining useful life prediction of lithium-ion batteries based on false nearest neighbors and a hybrid neural network, *Applied Energy*, vol. 253, art. no. 113626, 2019.

[30] H. Meng and Y.-F. Li, A review on prognostics and health management (PHM) methods of lithium-ion batteries, *Renewable and Sustainable Energy Reviews*, vol. 116, art. no. 109405, 2019.

[31] Q. Miao, L. Xie, H. Cui, W. Liang, and M. Pecht, Remaining useful life prediction of lithium-ion battery with unscented particle filter technique, *Microelectronics Reliability*, vol. 53, no. 6, pp. 805-810, 2013.

[32] S. S. Ng, Y. Xing, and K. L. Tsui, A naive Bayes model for robust remaining useful life prediction of lithium-ion battery, *Applied Energy*, vol. 118, pp. 114-123, 2014.

[33] S. Paradis and M. Whitmeyer, Pay attention: Leveraging sequence models to predict the useful life of batteries, *arXiv preprint arXiv: 1910.01347*, 2019.

[34] C. Pillot, The rechargeable battery market and main trends 2018-2030, In: *Proceedings of the 24th International Congress for Battery Recycling*, Lyon, France, Sept. 2019.

[35] X. Qiu, W. Wu, and S. Wang, Remaining useful life prediction of lithium-ion battery based on improved cuckoo search particle filter and a novel state of charge estimation method, *Journal of Power Sources*, vol. 450, art. no. 227700, 2020.

[36] F. Qu, X. Zhao, X. Wang, and E. Tian, Probabilistic-constrained distributed fusion filtering for a class of time-varying systems over sensor networks: A torus-event-triggering mechanism, *International Journal of Systems Science*, vol. 53, no. 6, pp. 1288-1297, 2022.

[37] I. Sergey and S. Christian, Batch normalization: Accelerating deep network training by reducing internal covariate shift, *arXiv preprint arXiv: 1502.03167*, 2015.

[38] K. A. Severson, P. M. Attia, N. Jin, N. Perkins, B. Jiang, Z. Yang, M. H. Chen, M. Aykol, P. K. Herring, D. Fraggedakis, M. Z. Bazant, S. J. Harris, W. C. Chueh, and R. D. Braatz, Data-driven prediction of battery cycle life before capacity degradation, *Nature Energy*, vol. 4, no. 5, pp. 383-391, 2019.

[39] M. Sheng, Z. Wang, W. Liu, X. Wang, S. Chen, and X. Liu, A particle swarm optimizer with multi-level population sampling and dynamic p-learning mechanisms for large-scale optimization, *Knowledge-Based Systems*, vol. 242, art. no. 108382, 2022.

[40] B. Song, H. Miao, and L. Xu, Path planning for coal mine robot via improved ant colony optimization algorithm, *Systems Science & Control Engineering*, vol. 9, no. 1, pp. 283-289, 2021.

[41] J. Tian, R. Xu, Y. Wang, and Z. Chen, Capacity attenuation mechanism modeling and health assessment of lithium-ion batteries, *Energy*, vol. 221, art. no. 119682, 2021.

[42] Y. Wang, J. Tian, Z. Sun, L. Wang, R. Xu, M. Li, and Z. Chen, A comprehensive review of battery modeling and state estimation approaches for advanced battery management systems, *Renewable and Sustainable Energy Reviews*, vol. 131, art. no. 110015, 2020.

[43] L. Xu, B. Song, and M. Cao, A new approach to optimal smooth path planning of mobile robots with continuous-curvature constraint, *Systems Science & Control Engineering*, vol. 9, no. 1, pp. 138-149, 2021.

[44] Z. Xue, Y. Zhang, C. Cheng, and G. Ma, Remaining useful life prediction of lithium-ion batteries with adaptive unscented kalman filter and optimized support vector regression, *Neurocomputing*, vol. 376, pp. 95-102, 2020.

[45] Z. Yang, Y. Liu, W. Zhang, F. E. Alsaadi, and K. H. Alharbi, Differentially private containment control for multi-agent systems, *International Journal of Systems Science*, in press, DOI: 10.1080/00207721.2022.2070794.

[46] Y. Yuan, G. Ma, C. Cheng, B. Zhou, H. Zhao, H.-T. Zhang, and H. Ding, A general end-to-end diagnosis framework for manufacturing systems, *National Science Review*, vol. 7, no. 2, pp. 418-429, 2020.

[47] W. Yue, Z. Wang, B. Tian, A. Payne, and X. Liu, A collaborative-filtering-based data collection strategy for Friedreich's ataxia, *Cognitive Computation*, vol. 12, no. 1, pp. 249-260, 2020.

[48] Y. Zhang, Q. Tang, Y. Zhang, J. Wang, U. Stimming, and A. A. Lee, Identifying degradation patterns of lithium ion batteries from impedance spectroscopy using machine learning, *Nature Communications*, vol. 11, art. no. 1706, 2020.

[49] Y. Zhang, L. Tu, Z. Xue, S. Li, L. Tian, and X. Zheng, Weight optimized unscented Kalman filter for degradation trend prediction of lithium-ion battery with error compensation strategy, *Energy*, vol. 251, art. no. 123890, 2022.

[50] Y. Zhang, Y. Xin, Z. Liu, M. Chi, and G. Ma, Health status assessment and remaining useful life prediction of aero-engine based on BiGRU and MMoE, *Reliability Engineering & System Safety*, vol. 220, art. no. 108263, 2022.

[51] Y. Zhang, R. Xiong, H. He, and M. Pecht, Validation and verification of a hybrid method for remaining useful life prediction of lithium-ion batteries, *Journal of Cleaner Production*, vol. 212, pp. 240-249, 2019.

[52] Y. Zhang, R. Xiong, H. He, and M. G. Pecht, Long short-term memory recurrent neural network for remaining useful life prediction of lithium-ion batteries, *IEEE Transactions on Vehicular Technology*, vol. 67, no. 7, pp. 5695-5705, 2018.

[53] Y. Zhang, R. Xiong, H. He, and M. G. Pecht, Lithium-ion battery remaining useful life prediction with Box-Cox transformation and Monte Carlo simulation, *IEEE Transactions on Industrial Electronics*, vol. 66, no. 2, pp. 1585-1597, 2018.

[54] Q. Zhao, X. Qin, H. Zhao, and W. Feng, A novel prediction method based on the support vector regression for the remaining useful life of lithium-ion batteries, *Microelectronics Reliability*, vol. 85, pp. 99-108, 2018.

[55] Z. Zhao, W. Qian, and X. Xu, Stability analysis for delayed neural networks based on a generalized free-weighting matrix integral inequality, *Systems Science & Control Engineering*, vol. 9, no. s1, pp. 6-13, 2021.

[56] Y. Zhou and M. Huang, Lithium-ion batteries remaining useful life prediction based on a mixture of empirical mode decomposition and ARIMA model, *Microelectronics Reliability*, vol. 65, pp. 265-273, 2016.